Sonderforschungsbereich 438

Mathematische Modellierung, Simulation und Verifikation
in materialorientierten Prozessen und intelligenten Systemen

Modeling, Simulation, and Control of Electrorheological Fluid Devices

Hoppe, Ronald H. W.; Mazurkevitch, George;
Rettig, Uwe; von Stryk, Oskar

Preprint SFB-438-9917

September 99

Technische Universität München Universität Augsburg

Cataloging Data :

Hoppe, Ronald H. W.; Mazurkevitch, George; Rettig, Uwe; von Stryk, Oskar: Modeling, Simulation, and Control of Electrorheological Fluid Devices; Sonderforschungsbereich 438: Technische Universität München, Universität Augsburg; Preprint SFB-438-9917(99)

Mathematics Subject Classification : 34H05 76A05

Editor :

K.H. Hoffmann (hoffmann@appl-math.tu-muenchen.de),
Technische Universität München, D-80290 München, Germany.

For the Electronic Version see : http://www-lit.mathematik.tu-muenchen.de/reports/html/SFB/

Modeling, Simulation, and Control of Electrorheological Fluid Devices

Ronald H. W. Hoppe[1], George Mazurkevitch[1], Uwe Rettig[2], and Oskar von Stryk[2]

[1] University of Augsburg, Inst. of. Math., D-86159 Augsburg, Germany
[2] Technische Universität München, Chair M2 Numerische Mathematik, D-80290 München, Germany

Dedicated to Karl-Heinz Hoffmann on the occasion of his 60th birthday

Abstract. The new generation of electrorheological fluids (ERFs) offers a wide range of applicability in fluid mechatronics with automotive ERF devices such as ERF shock absorbers mentioned at first place. The optimal design of such tools requires the proper modelling and simulation both of the operational behavior of the device itself as well as its impact on the dynamics of the complete vehicle. This paper addresses these issues featuring an extended Bingham fluid model and its numerical solution as well as substitutive models of viscoeleastic-plastic system behavior. Also control issues for optimal active suspension of vehicles with controllable ERF shock absorbers are discussed.

1 Introduction

Electrorheological fluids (ERFs) are microstructured fluids consisting of a dispersion of electrically polarizable particles in a nonconducting liquid. The characteristic feature is that under the influence of an outer electric field the initially unordered particles get oriented and stick together to form particle chains in the fluid. On the macroscopic scale this process results in a significant increase of the dynamic viscosity of the ERF yielding a considerable increase of the shear stress (cf., e.g., [9,10,32], and [38]). Therefore, ERFs are highly amenable to an efficient control of the transmission of forces. They are thus potentially useful for applications in hydraulic systems and automotive devices such as clutches, engine bearings, and shock absorbers (cf., e.g., [15–17,20,21], and [39]). The new generation of ERFs which has been developed in recent years features high ER effects by direct activation through electrical signals with an adaptation of the forces in the range of milliseconds that goes along with low abrasive wear, good redispersibility and high shear stress and sedimentation stability (see [5,3], and [37]). Despite this progress, ERFs are not yet used in mass production due to still existing problems, as for instance a stable operational behavior over a wide range of temperatures or their interaction with other components of the devices such as the power supply. Nevertheless, it can be foreseen that the rapid development of ongoing research will put them into the marketplace within only a few years. The optimal design and layout of individual ERF devices is one important aspect.

Another equally important one is to study their behavior, in particular their controllability, as an integral part of a complete system.

It is the purpose of this paper to provide mathematical tools for modeling and simulation of both the fluid flow in specific ERF devices within a continuum mechanical framework and the dynamical behavior of such devices as integral parts in mechatronical vehicle systems based on the description of the vehicle as a multibody system. The issue of an efficient control of ERF dampers for active suspension of vehicles is also addressed.

The paper is organized as follows: After these introductory remarks, in Sect. 2.1 we will begin with a brief overview on the basic modes of fluid flows in ERF devices. As far as the modelling aspect is concerned, in Sect. 2.2 we present an extension of the classical Bingham fluid model that goes beyond pure shear or flow modes and is thus able to describe the flow pattern in complete devices. In Sect. 2.3 we elaborate in some detail on the method of augmented Lagrangians combined with operator splitting techniques that is based on a primal-dual formulation of the problem and can efficiently handle the inherent nonlinearities. This is followed by a documentation of numerical simulation results for shear and flow modes in ERF devices given in Sect. 2.4. Geometric design aspects of ERF shock absorbers are mentioned in Sect. 3.1 and followed in Sect. 3.2 by a discussion of substitutive models for the viscoelastic-plastic system behavior. Optimal and robust optimal feedback controllers for optimal active suspension of a quarter car model based on LQR and H^∞ techniques are investigated in Sect. 3.3. Numerical results are presented in Sect. 3.4.

2 Modeling and Simulation of ERF flows

2.1 Modes of Fluid Flows in ERF devices

In applications of ERFs in automotive devices there are basically three different types of fluid modes: the shear mode, the flow mode, and the squeeze mode.

The shear mode occurs when the electrodes are sheared against each other, as for instance in clutches. A simple model of an ER clutch is shown in Fig. 1. The ERF is located in a housing consisting of two coaxial cylinders with the inner one being driven at some constant angular speed. The inner cylinder hosts a high voltage lead supplying the lateral surface serving as the electrode whereas the lateral surface of the outer cylinder acts as the output. If voltage is applied to the electrodes, an electric field builds up which in the gap between the cylinders is perpendicular to the Couette type flow. The viscosity of the ERF increases with increasing electric field strength as does the torque exerted on the outer cylinder.

The flow mode is predominant in devices where the ERF passes through ducts with fixed electrodes such as shock absorbers or engine mounts. Fig. 1 displays the longitudinal section of a cylindrical shock absorber featuring two

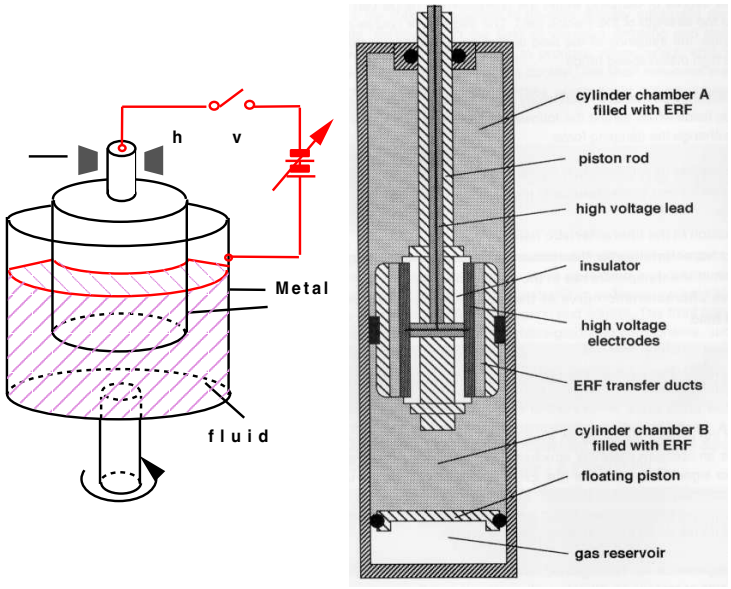

Fig. 1. Schematical representation of an ERF clutch (left) and ERF shock absorber (right) (cf. [7])

ERF-filled chambers with a piston in between that contains two tranfer ducts. There is a third gas-filled chamber separated from the others by a floating piston. The inner walls of the ducts serve as electrodes that are supplied by a voltage lead within the piston rod. In the ducts the generated electric field is perpendicular to the Poiseuille type flow of the ERF.

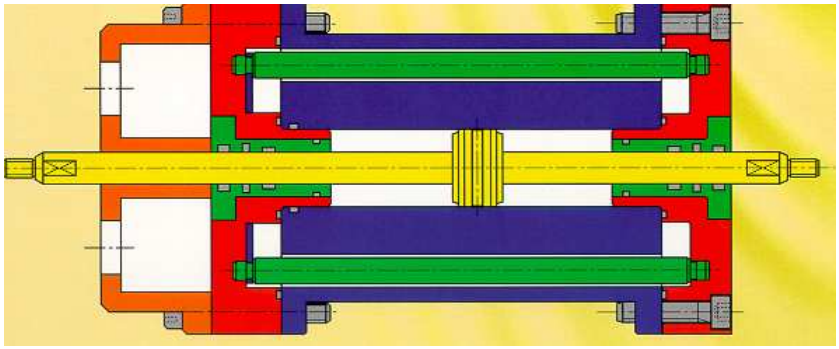

Fig. 2. ERF actuator (cf. [6])

A third type of mode, the so-called squeeze mode, prevails in ERF actuators used, for instance, as vibration dampers. In this case the electrodes are subjected to vibrations so that the ERF is either pressed out of the gap between the electrodes or sucked into it (cf. Fig. 3 for a schematic representation of an industrially produced ERF actuator).

2.2 The Extended Bingham Fluid Model

The flow of an ERF can be modelled by a coupled system of PDEs consisting of a second order elliptic equation for the potential of the electric field and an extension of the classical Bingham fluid model that goes beyond pure shear mode or flow mode and thus allows to determine the fluid flow in the complete device (cf., e.g., [14]).

Denoting by $\Omega \subset \mathbf{R}^d$, $d \in \mathbf{N}$ the physical domain, i.e., the region filled with the ERF, we have

$$\rho(\frac{\partial \mathbf{u}}{\partial t} + (\mathbf{u} \cdot \nabla)\mathbf{u}) \in \nabla \cdot \sigma(\mathbf{u}, \mathbf{E}) \quad \text{in } \Omega \tag{1}$$

$$\nabla \cdot \mathbf{u} = 0 \quad \text{in } \Omega \tag{2}$$

where the stress tensor $\sigma = \partial \mathcal{D}$ is the subgradient of the (local) energy functional

$$\mathcal{D}(\mathbf{u}, \mathbf{E}) := -\nabla p + \gamma \mid \mathbf{E} \mid \mid \mathbf{D}(\mathbf{u})\mathbf{E} \mid + \frac{\eta}{2}\|\mathbf{D}(\mathbf{u})\|_F^2 \ . \tag{3}$$

Here, $\mathbf{u} := (u_1, ..., u_d)^T$ stands for the velocity field, $\mathbf{D}(\mathbf{u}) := \frac{1}{2}(\nabla \mathbf{u} + (\nabla \mathbf{u})^T)$ is the rate of deformation tensor, $\mathbf{E} := (E_1, E_2, E_3)^T$ is the electric field, $-p\mathbf{I}$ denotes the spherical part of the stress tensor so that p can be interpreted as the pressure and $\|\cdot\|_F$ refers to the Frobenius norm of a matrix. Moreover, ρ, η and γ are material parameters with ρ and η being the density and zero field viscosity of the ERF, respectively, whereas γ is the proportionality factor in the quadratic dependence ($\sigma_E := \gamma \mid \mathbf{E} \mid^2$) of the yield limit on the electric field.

The stress tensor is not well defined if $\mid \mathbf{D}(\mathbf{u})\mathbf{E} \mid = 0$ which indicates the rigid zone. For an increasing electric field $\mathbf{E}$ the rigid zones grow and can completely block the flow for $\mid \mathbf{E} \mid$ sufficiently large.

Note that (1), (2) have to be interpreted in a weak sense. For instance, if we prescribe the tangential component $\mathbf{t} \cdot \mathbf{u}$ of the velocity on some part $\Gamma_t \subset \Gamma := \partial\Omega$ and impose no slip boundary conditions $\mathbf{n} \cdot \mathbf{u} = 0$ on all of Γ, an appropriate variational setting is provided by the function spaces

$$\mathbf{V} := \{\mathbf{v} \in H^1(\Omega)^d \mid \mathbf{t} \cdot \mathbf{v} \mid_{\Gamma_t} = u_t \ , \ \mathbf{n} \cdot \mathbf{v} \mid_{\Gamma} = 0\} \ ,$$

$$\mathbf{V}^0 := \{\mathbf{v} \in \mathbf{V} \mid \nabla \cdot \mathbf{v} = 0\} \quad , \quad \mathbf{V}_0^0 := \{\mathbf{v} \in H_0^1(\Omega) \mid \nabla \cdot \mathbf{v} = 0\} \ .$$

In particular, the variational formulation of the flow problem amounts to the solution of the parabolic variational inequality:
Find $\mathbf{u} \in L^2(0,T;\mathbf{V}_0^0) \cap L^\infty(0,T;\mathbf{V}_0)$, $\partial\mathbf{u}/\partial t \in L^2(0,T;(\mathbf{V}_0^0)^*)$ such that for all $\mathbf{v} \in \mathbf{V}_0^0$ and almost all $t \in (0,T]$

$$\int_\Omega \rho(\frac{\partial \mathbf{u}}{\partial t} + (\mathbf{u}\cdot\nabla)\mathbf{u})\cdot(\mathbf{v}-\mathbf{u})d\mathbf{x} + \int_\Omega \mathcal{D}(\mathbf{v},\mathbf{E})d\mathbf{x} - \int_\Omega \mathcal{D}(\mathbf{u},\mathbf{E})d\mathbf{x} \geq 0 . \tag{4}$$

We remark that (4) admits a unique solution if $d = 2$ (cf., e.g., [12,19]).

The electric field $\mathbf{E}$ is generated by some voltage U applied to an electrode Γ_e that is part of the boundary whereas the opposite counterelectrode Γ_c is voltage free. Observing $\mathbf{E} = -\varepsilon\nabla\varphi$ where φ is the electric potential and ε refers to the permeability of the ERF, the potential can be obtained as the solution of the elliptic boundary value problem

$$-\nabla\cdot\varepsilon\nabla\varphi = 0 \quad \text{in } \Omega , \tag{5}$$

$$\varphi = U \text{ on } \Gamma_e , \quad \varphi = 0 \text{ on } \Gamma_c , \quad \mathbf{n}\cdot\varepsilon\nabla\varphi = 0 \text{ on } \Gamma\setminus(\Gamma_e\cup\Gamma_c) . \tag{6}$$

Setting $V := \{\psi \in H^1(\Omega) \mid \psi|_{\Gamma_e\cup\Gamma_c} = 0\}$, the variational formulation of (4,5) is to find $\varphi \in H^1(\Omega)$, $\varphi\,|_{\Gamma_e} = U$, $\varphi\,|_{\Gamma_c} = 0$ such that

$$\int_\Omega \sigma\nabla\varphi\cdot\nabla\psi d\mathbf{x} = 0 , \quad \psi \in V . \tag{7}$$

2.3 The Method of Augmented Lagrangians

The difficulty associated with the inherent nonlinearity in (4) can be circumvented by applying the method of augmented Lagrangians. Combined with an appropriate operator splitting technique this confines the nonlinearity to local, low-dimensional problems (cf., e.g., [18,19]).

We discretize (4) implicitly in time by the backward Euler scheme with respect to a partition $0 =: t_0 < t_1 < \ldots < t_M := T$ of the time interval $[0,T]$ resulting in elliptic type variational inequalities that have to be solved at each time level $t_m := t_{m-1} + (\Delta t)_m$, $1 \leq m \leq M$:
Find $\mathbf{u}^m \in \mathbf{V}^0$ such that for all $\mathbf{v} \in \mathbf{V}_0^0$

$$\rho\int_\Omega \mathbf{u}^m\cdot(\mathbf{v}-\mathbf{u}^m)d\mathbf{x} + \rho(\Delta t)_m\int_\Omega (\mathbf{u}^m\cdot\nabla)\mathbf{u}^m\cdot(\mathbf{v}-\mathbf{u}^m)d\mathbf{x} + \tag{8}$$

$$+ (\Delta t)_m(\int_\Omega \mathcal{D}(\mathbf{v},\mathbf{E})d\mathbf{x} - \int_\Omega \mathcal{D}(\mathbf{u}^m,\mathbf{E})d\mathbf{x}) \geq \rho\int_\Omega \mathbf{u}^{m-1}\cdot(\mathbf{v}-\mathbf{u}^m)d\mathbf{x} .$$

The method of augmented Lagrangians is applied to (8) based on a primal-dual formulation by introducing $\mathbf{p}_i := \nabla u_i^m$, $1 \leq i \leq d$, as additional variables and by coupling the constraints $\mathbf{p}_i - \nabla u_i^m = \mathbf{0}$, $1 \leq i \leq d$, as well as the incompressibility constraint $\nabla \cdot \mathbf{u}^m = 0$ both by Lagrangian multipliers and penalty terms.

Setting $\mathbf{f} := \rho \mathbf{u}^{m-1} - (\Delta t)_m \nabla p$, introducing the matrix-valued functions $\mathbf{P} := (\mathbf{p}_1 \mid ... \mid \mathbf{p}_d)$, $\boldsymbol{\lambda} := (\lambda_1 \mid ... \mid \lambda_d)$, where $\mathbf{p}_i, \lambda_i \in L^2(\Omega)^d$, $1 \leq i \leq d$, and given penalization parameters $\boldsymbol{\kappa} := (\kappa_1, \kappa_2)^T$ with $\kappa_\nu > 0, 1 \leq \nu \leq 2$, we are thus led to the saddle point problem:

Find $(\mathbf{u}^m, \mathbf{P}, \boldsymbol{\lambda}, \theta) \in \mathbf{V} \times L^2(\Omega)^{d \times d} \times L^2(\Omega)^{d \times d} \times L^2(\Omega)$ such that

$$L_{\boldsymbol{\kappa}}(\mathbf{u}^m, \mathbf{P}, \boldsymbol{\lambda}, \theta) \;=\; \inf_{\mathbf{v}, \mathbf{Q}} \sup_{\boldsymbol{\mu}, \tau} L_{\boldsymbol{\kappa}}(\mathbf{v}, \mathbf{Q}, \boldsymbol{\mu}, \tau) \;. \tag{9}$$

The Lagrangian $L_{\boldsymbol{\kappa}}$ is given by

$$L_{\boldsymbol{\kappa}}(\mathbf{v}, \mathbf{Q}, \boldsymbol{\mu}, \tau) := \rho(\Delta t)_m \int_\Omega (\mathbf{Q} - \frac{1}{2}\mathrm{diag}\mathbf{Q})\mathbf{v} \cdot \mathbf{v} d\mathbf{x} + \gamma(\Delta t)_m \int_\Omega \mid \mathbf{E} \mid\mid \mathbf{Q}_s \mathbf{E} \mid d\mathbf{x}$$

$$+ \frac{\eta}{2}(\Delta t)_m \int_\Omega \|\mathbf{Q}_s\|_F^2 d\mathbf{x} + \frac{\rho}{2} \int_\Omega \mid \mathbf{v} \mid^2 d\mathbf{x} - \int_\Omega \mathbf{f} \cdot \mathbf{v} d\mathbf{x} + \sum_{i=1}^{d} \int_\Omega \mu_i \cdot (\mathbf{q}_i - \nabla v_i) d\mathbf{x}$$

$$+ \int_\Omega \tau \nabla \cdot \mathbf{v} d\mathbf{x} + \frac{\kappa_1}{2} \sum_{i=1}^{d} \int_\Omega \mid \mathbf{q}_i - \nabla v_i \mid^2 d\mathbf{x} + \frac{\kappa_2}{2} \int_\Omega \mid \nabla \cdot \mathbf{v} \mid^2 d\mathbf{x}$$

where $\mathbf{Q}_s := \frac{1}{2}(\mathbf{Q} + \mathbf{Q}^T)$.

As far as the discretization in space is concerned, we assume a simplicial triangulation $\mathcal{T}_h$ of Ω and approximate the velocities u_i, $1 \leq i \leq d$, by continuous, piecewise linear finite elements augmented by cubic bubble functions associated with each element of $\mathcal{T}_h$. We denote by $S_1(\Omega; \mathcal{T}_h)$ the conforming P1 finite element space and by $B_3(\Omega; \mathcal{T}_h) := \mathrm{span}\{\prod_{i=1}^{d+1} \lambda_i^T \mid T \in \mathcal{T}_h\}$ the linear space of cubic bubbles where λ_i^T, $1 \leq i \leq d+1$, are the barycentric coordinates associated with $T \in \mathcal{T}_h$. We set

$$\mathbf{V}_h \;:=\; V_h^d \quad , \quad V_h \;:=\; S_1(\Omega; \mathcal{T}_h) \oplus B_3(\Omega; \mathcal{T}_h) \;. \tag{10}$$

The components p_{ij}, λ_{ij}, $1 \leq i, j \leq d$, of the variables $\mathbf{p}_i$, $1 \leq i \leq d$, and the multipliers $\boldsymbol{\lambda}_i$, $1 \leq i \leq d$, as well as the multiplier θ will be approximated by elementwise constants, i.e., we define

$$\mathbf{W}_h \;:=\; W_h^d \quad , \quad W_h \;:=\; \{w_h \in L^2(\Omega) \mid w_h \mid_T \in P_0(T), T \in \mathcal{T}_h\} \;. \tag{11}$$

Then, the discretized saddle point problem reads as follows:

Find $(\mathbf{u}_h, \mathbf{P}_h, \boldsymbol{\lambda}_h, \theta_h) \in \mathbf{V}_h \times \mathbf{W}_h^d \times \mathbf{W}_h^d \times \mathbf{W}_h$ such that

$$L_{\boldsymbol{\kappa}}(\mathbf{u}_h, \mathbf{P}_h, \boldsymbol{\lambda}_h, \theta_h) \;=\; \inf_{\mathbf{v}_h, \mathbf{Q}_h} \sup_{\boldsymbol{\mu}_h, \tau_h} L_{\boldsymbol{\kappa}}(\mathbf{v}_h, \mathbf{Q}_h, \boldsymbol{\mu}_h, \tau_h) \;. \tag{12}$$

Note that (12) satisfies the Ladyzhenskaja-Babuska-Brezzi (LBB-) condition and is thus well-defined.

We will solve (12) by an iterative procedure that is based on operator splitting techniques. Each iteration consists of two steps. The first one requires the subsequent solution of global linear problems whereas the second one involves the solution of local, low-dimensional nonlinear problems.

We assume that we are given initial values $u_i^0 \in V_h, 2 \le i \le d,\;\; \mathbf{p}_i^0 \in \mathbf{W}_h$, $\lambda_i^1 \in \mathbf{W}_h, 1 \le i \le d, \theta^1 \in W_h$ and sequences $(\kappa_\nu^n)_{\mathbf{N}}, (\rho_\nu^n)_{\mathbf{N}}, 1 \le \nu \le 2$, of penalization parameters $\kappa_\nu^n > 0$ and update parameters $\rho_\nu^n > 0, 1 \le \nu \le 2, n \in \mathbf{N}$. For notational convenience we have dropped the super- resp. subscripts h and m for the independent variables. Then, for $n \in \mathbf{N}$ we perform the following iteration steps:

Step 1: For $i = 1, .., d$ compute $u_i^n \in V_h$ as the solution of the minimization problem

$$L_{\boldsymbol{\kappa}}(u_1^n, ..., u_{i-1}^n, u_i^n, u_{i+1}^{n-1}, ..., u_d^{n-1}, \mathbf{P}^{n-1}, \boldsymbol{\lambda}^n, \theta^n) \;= \tag{13}$$

$$= \inf_{v_i \in V_h} L_{\boldsymbol{\kappa}}(u_1^n, ..., u_{i-1}^n, v_i, u_{i+1}^{n-1}, ..., u_d^{n-1}, \mathbf{P}^{n-1}, \boldsymbol{\lambda}^n, \theta^n)$$

and update the multiplier λ_i according to

$$\lambda_i^{n+\frac{1}{2}} \;=\; \lambda_i^n \;+\; \rho_1^n (\nabla u_i^n \;-\; \mathbf{p}_i^{n-1}) \;. \tag{14}$$

Finally, update the multiplier θ

$$\theta^{n+1} \;=\; \theta^n \;+\; \rho_2^n \nabla \cdot \mathbf{u}^n \;. \tag{15}$$

Step 2: For $i = 1, .., d$ compute $\mathbf{p}_i^n \in \mathbf{W}_h$ by solving the elementwise nonlinear minimization problems

$$L_{\boldsymbol{\kappa}}^T(\mathbf{u}^n, \mathbf{p}_1^n, ..., \mathbf{p}_{i-1}^n, \mathbf{p}_i^n, \mathbf{p}_{i+1}^{n-1}, ..., \mathbf{p}_d^{n-1}, \boldsymbol{\lambda}^{n+\frac{1}{2}}, \theta^{n+1}) \;= \tag{16}$$

$$= \inf_{\mathbf{q}_i \in \mathbf{W}_h} L_{\boldsymbol{\kappa}}^T(\mathbf{u}^n, \mathbf{p}_1^n, ..., \mathbf{p}_{i-1}^n, \mathbf{q}_i, \mathbf{p}_{i+1}^{n-1}, ..., \mathbf{p}_d^{n-1}, \boldsymbol{\lambda}^{n+\frac{1}{2}}, \theta^{n+1}) \;,\; T \in \mathcal{T}_h \;.$$

where $L_{\boldsymbol{\kappa}}^T$ denotes the Lagrangian $L_{\boldsymbol{\kappa}}$ restricted to $T \in \mathcal{T}_h$.

Update the multiplier λ_i according to

$$\lambda_i^{n+1} \;=\; \lambda_i^{n+\frac{1}{2}} \;+\; \rho_1^n (\nabla u_i^n \;-\; \mathbf{p}_i^n) \;. \tag{17}$$

Remarks: The computation of $u_i^n \in V_h, 1 \leq i \leq d$, in the first step requires the solution of the following variational equations

$$\sum_{j=1}^{d} \int_\Omega (\kappa_1^n \frac{\partial u_i^n}{\partial x_j} + \kappa_2^n \frac{\partial u_i^n}{\partial x_j} \delta_{ij}) \frac{\partial v}{\partial x_j} d\mathbf{x} + \rho \int_\Omega u_i^n v \, d\mathbf{x} + \Delta t \rho \int_\Omega p_{ii}^{n-1} u_i^n v \, d\mathbf{x} =$$

$$= \int_\Omega f_i v \, d\mathbf{x} - \Delta t \rho \int_\Omega \left(\sum_{j=1}^{i-1} (p_{ij}^{n-1} + p_{ji}^{n-1}) u_j^n + \sum_{j=i+1}^{d} (p_{ij}^{n-1} + p_{ji}^{n-1}) u_j^{n-1} \right) d\mathbf{x} +$$

$$+ \int_\Omega \lambda_i^n \cdot \nabla v \, d\mathbf{x} + \kappa_1^n \int_\Omega \mathbf{p}_i^{n-1} \cdot \nabla v \, d\mathbf{x} - \int_\Omega \theta^n \frac{\partial v}{\partial x_i} d\mathbf{x} -$$

$$-\kappa_2^n \int_\Omega \left(\sum_{j=1}^{i-1} \frac{\partial u_j^n}{\partial x_j} \frac{\partial v}{\partial x_i} + \sum_{j=i+1}^{d} \frac{\partial u_j^{n-1}}{\partial x_j} \frac{\partial v}{\partial x_i} \right) d\mathbf{x} \quad , \quad v \in V_h \ .$$

For the computation of $\mathbf{p}_i^n \mid_T \in P_0(T)^d, 1 \leq i \leq d, T \in \mathcal{T}_h$, in the second step we have to solve d-dimensional minimization problems in the unknowns $p_{ij}^n \mid_T \in P_0(T), 1 \leq j \leq d$, which can be done by Newton's method applied to the first order optimality conditions.

2.4 Simulation Results

Based on the extended Bingham fluid model and its numerical solution by the method of augmented Lagrangians as described in the previous sections we have performed simulations of an ERF clutch and an ERF shock absorber (cf. Fig. 1).

In particular, for a clutch with the radii $r_i = 3.5\,cm$, $r_e = 7.0\,cm$ and lengths $\ell_i = 25.0\,cm$, $\ell_e = 30.0\,cm$ of the inner resp. outer cylinder, an angular velocity of $125\,rads^{-1}$ of the inner cylinder, and an ERF with $\eta = 0.9 \cdot 10^{-1}\,kgm^{-1}s^{-1}$, $\gamma = 1.0 \cdot 10^{-9}\,PaV^{-2}$ the Figures 3 and 4 display the adaptively generated computational grids and velocity distributions (see Fig. 4) and the angular velocity profiles between the inner and outer cylinder (see Fig. 3) for different applied voltages. For a detailed discussion and more results as e.g. the torque on the outer cylinder as a function of the applied voltage we refer to [14].

On the other hand, for an ERF shock absorber with a geometry of the fluid chamber as shown in Fig. 1 and an ERF with the same characteristics as for the ERF clutch, Fig. 5 (left) shows the equipotential lines of the electrostatic potential in case of an applied voltage of $U = 1000\ V$ whereas Fig. 5 (right) represents the velocity distribution in the chamber for a velocity $u_t = 0.001\ ms^{-1}$ of the piston and a pressure difference of $\Delta p = 0.0\ Nm^{-2}$ between the inflow and outflow boundaries.

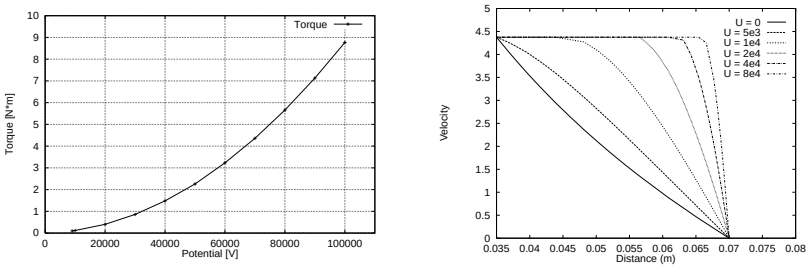

Fig. 3. Torque as a function of applied voltage (left), Angular velocity profiles for different values of potential (right)

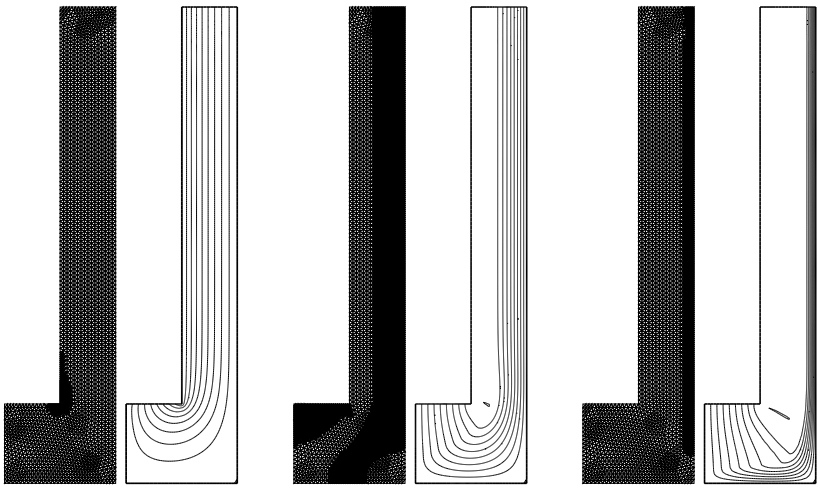

Fig. 4. Computational grids and velocity distribution for $U = 0$V (left), $U = 1{\cdot}10^4$V (middle) and $U = 4 \cdot 10^4$V (right)

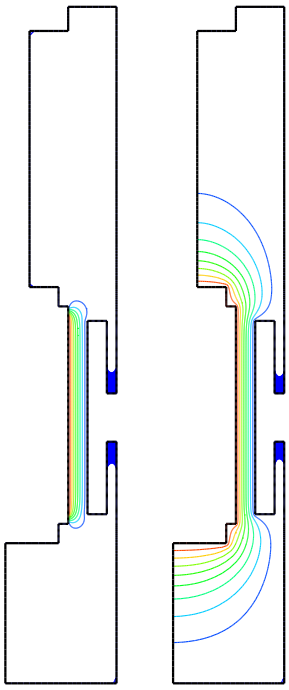

Fig. 5. Potential and z-component of velocity

3 Modeling, Simulation, and Control of ERF Dampers for Active Vehicle Suspension

Models of ERF shock absorbers suitable for control purposes are investigated in this section. However, due to their qualitatively similar behaviour phenomenological models of electro- and magnetorheological (MR) fluid devices can mostly be applied to either material [23].

3.1 Design Aspects of Electrorheological Fluid Dampers

Typical geometric designs of dampers with controllable electrorheological or magnetorheological fluids for use as automotive shock absorbers are displayed in Fig. 6. The piston rod which moves up and down in a chamber filled with the ERF may be one- or double-sided (Figs. 6(b), 6(a)). The cylinder may be equipped with a bypass to enable fluid flow between the separated upper and the lower parts of the chamber (Fig. 6(c)). However, ERF dampers with

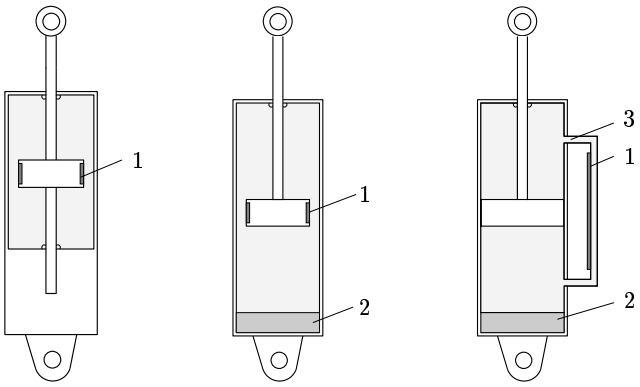

Fig. 6. ERF damper geometries (1 - field generator, 2 - accumulator, 3 - bypass).

double sided piston rod are longer and require more space than dampers equipped with one sided piston rods and equivalent performance. Thus, they are less suited for automotive applications. Dampers designed with a bypass also require more space than without one.

The accumulator (Figs. 6(b), 6(c)) compensates the change in volume of the fluid caused by movements of the piston rod and by thermal expansion. It prevents cavitation while the pressure amounts about 20 bar. Hence, the accumulator affects the dynamical behavior of the ERF damper – from a phenomenological point of view – like a spring.

For the optimal design and application of ERF dampers for active suspension of vehicles mathematical models are needed taking into account the nonlinear dynamic behavior of the damper and the vehicle. The purpose of numerical simulation is to reproduce and to predict the behavior of the damper to investigate the performance of various damper designs and to design the best possible control for a specific application. The characteristic damper properties include the *force-velocity* (Fig. 7) as well as the *force-displacement* relations.

Numerical fluid simulation in complex three-dimensional geometries is computationally too expensive for control purposes where hundreds or thousands of situations must be investigated quickly during the simulated or experimentally conducted ride of a vehicle. However, the accurate simulation of the ERF flow inside the chambers is needed for investigating the performance of various ERF damper designs and for providing reference data to calibrate the parameters of a phenomenological model of the ERF damper dynamics.

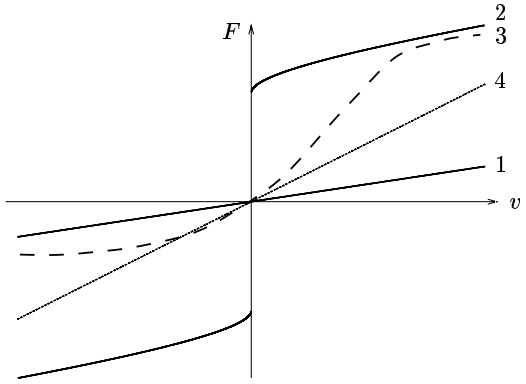

Fig. 7. Typical force-velocity relation of an ERF shock absorber at constant minimum (1) and constant maximum (2) field strengths and for varying field strengths (3) compared to a conventional, passive shock absorber (4).

The performance of an ERF damper depends on the geometric design as well as on the properties of the used ERF. The spectrum of the yield point of the fluid depends on the electric field strength and is of significant importance for shock absorbing and control properties. Fig. 7 shows typical force-velocity relations for a conventional and an ERF shock absorber. The force-velocity relation of the ERF damper depends on the shear stress versus shear strain rate relation of the ERF. The design of an adaptively controllable ERF damper must take into account that the curves for constant minimum and maximum field strengths must span the region of all desired damping rates (Fig. 7). The larger the enclosed region of possible damping curves the

higher the ERF requirements. While the ERF properties are mainly responsible for the width of the area of possible force-velocity curves and for the slopes of the envelopes, the geometric design determines the relation between bandwidth and slope.

3.2 Phenomenological Models of ERF Dampers

The geometry to be considered for the computation of the fluid flow within an ERF shock absorber without bypass and with a one sided piston rod (Fig. 6(b)) is less complicated than in a damper with bypass (cf. Sect. 2.1). The fluid flow in the region between the inner piston head and the main cylinder can be computed almost analytically if a Poiseuille type flow excited by a pressure difference between the lower and upper chambers is assumed. For a radial symmetric design, a constant electric field strength, perpendicular directions of the both fields, a constant flow velocity u within the gap and using radial symmetric coordinates, the PDEs investigated in Sect. 2.2 reduce to a steady state, one dimensional ordinary differential equation (ODE)

$$\frac{\mathrm{d}\tau}{\mathrm{d}r} + \frac{\tau}{r} = \frac{\Delta P}{L} \tag{18}$$

with a simple Bingham model

$$\begin{aligned} \tau &= \tau_0 \operatorname{sgn}\left(\frac{\mathrm{d}u}{\mathrm{d}r}\right) + \eta\frac{\mathrm{d}u}{\mathrm{d}r} && \text{if} \quad \tau > \tau_0, \\ \frac{\mathrm{d}u}{\mathrm{d}r} &= 0 && \text{if} \quad \tau < \tau_0. \end{aligned} \tag{19}$$

Here τ denotes the shear stress, τ_0 the yield point corresponding to the applied electric field strength, η the plastic viscosity as the slope of shear stress versus shear strain rate, r the radius with origin at the center of the cylinder. A linear pressure gradient along the piston head is denoted by $\Delta P/L$.

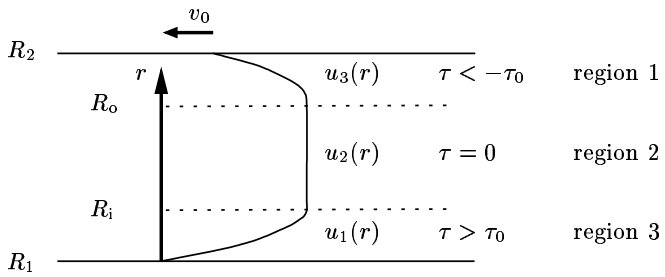

Fig. 8. Velocity field within the gap, $u(R_1) = v_0$, $u(R_2) = 0$.

The analytic solution of the ODE requires a separate treatment of the three regions of evolution of the shear stress (Fig. 8). Inside the inner region 2,

i.e., $R_\mathrm{i} \leq r \leq R_\mathrm{o}$, the velocity gradient vanishes and we obtain a plug flow region. If R_i and R_o would reach the boundary of the interval $[R_1, R_2]$ the gap would operate as a locked valve. If we consider the boundary conditions at $r = R_1, R_2$ and the transition conditions at $r = R_\mathrm{i}, R_\mathrm{o}$ we obtain (cf. [2,22])

$$u_1(r) = \frac{\Delta P}{4\eta L}\left[r^2 - R_1^2 - 2R_\mathrm{i}^2 \ln\left(\frac{r}{R_1}\right)\right] - \frac{\tau_0}{\eta}\left[r - R_1 - R_\mathrm{i}\ln\left(\frac{r}{R_1}\right)\right] - v_0$$

$$u_3(r) = \frac{\Delta P}{4\eta L}\left[r^2 - R_2^2 - 2R_\mathrm{o}^2 \ln\left(\frac{r}{R_2}\right)\right] - \frac{\tau_0}{\eta}\left[r - R_2 - R_\mathrm{o}\ln\left(\frac{r}{R_2}\right)\right] \quad (20)$$

$$u_2(r) = u_1(R_\mathrm{i}) \quad (= u_3(R_\mathrm{o}))\ .$$

The variables R_i, R_o and the piston head velocity v_0 define the velocity field $u(r)$. Thus, the volume flow through the electrode gap is

$$Q(R_\mathrm{i}, R_\mathrm{o}, v_0) = \int_{R_1}^{R_2} 2\pi r u(r)\,\mathrm{d}r\ . \quad (21)$$

On the other hand the volume replacement of the piston head determines the volume flow according to $Q = Av_0$, where A denotes the area of the piston head. This relation and the two transient conditions at $r = R_\mathrm{i}, R_\mathrm{o}$ lead to a system of three nonlinear equalities that define F, R_i, and R_o for a given velocity v_0. Considering the relation $F = -\Delta P/L$ we obtain

$$\begin{aligned} 0 &= \bar{Q}(R_\mathrm{i}, R_\mathrm{o}, \Delta P) - (A + \pi(R_\mathrm{i}^2 - R_1^2))v_0 \\ 0 &= u_1(R_\mathrm{i}) - u_3(R_\mathrm{o}) \\ 0 &= \Delta P(R_\mathrm{o} - R_\mathrm{i}) - 2L\tau_0 \end{aligned} \quad (22)$$

where $\bar{Q}$ denotes a rather lengthy term calculated by analytical evaluation of (21). Equation (22) can be solved numerically for v_0 applying Newton's method for given F. In numerical experiments convergence was obtained from feasible initial values within a few iterations. However, the iterates must be prevented from leaving the valid reagion, as a singularity occurs at $v_0 = 0$ corresponding to the "locking" of the valve.

The approach described so far relies on several strong assumptions. Inertia terms have been neglected, i.e., an oscillating excitation leads to a transient PDE. Furthermore, viscoelasticity of the ERF occurs at small shear strain rates, resp. small velocities of the piston rod. Model equations considering this kind of fluid flow are currently not available and difficult to derive. Viscoelasticity causes hysteresis not only in the force-displacement relation, but also in the force-velocity relation. This effect is related to elastic properties at small shear strain rates, which are kept in "memory" during the elastic phase. Complex considerations assume a "fading memory" effect [8]. In addition, the presence of the accumulator and other mechanical details of the shock absorber lead to further mutation of the input-output behavior.

A substitutive model of viscoelastic fluids which may be combined with the Bingham model is investigated next. Maxwell recognized that the equation

$$\tau + \frac{\eta}{G}\frac{\partial \tau}{\partial t} = \mu\dot{\gamma} \tag{23}$$

where $\dot{\gamma}$ specifies the shear strain rate, η and G denote the viscosity resp. the modulus of elasticity, contains both the ideas of Newtonian liquids and Hookian solids [8]. More general types of the Maxwell model are

$$\left(1 + \sum_{n=1}^{\infty} a_n \frac{\partial^n}{\partial t^n}\right) \tau_{ij} = \eta_0 \left(1 + \sum_{n=1}^{\infty} b_n \frac{\partial^n}{\partial t^n}\right) \gamma_{ij} \tag{24}$$

$$\tau = \sum_k \tau_k, \qquad \tau_k + \lambda_k \frac{\partial}{\partial t}\tau_k = \eta_k \dot{\gamma}_k \tag{25}$$

with appropriate constants. Equation (25) represents a linear combination of several Maxwell models. A special case of (24) follows with

$$\tau + p_1\dot{\tau} = q_1\dot{\gamma} + q_2\ddot{\gamma}\ . \tag{26}$$

If we compare with the substitutive models depicted in Figs. 9(b) and 9(c) we obtain for

$$\begin{aligned} \text{case (b)} \quad & p_1 = \frac{c_1 + c_2}{k}, \quad & q_1 = c_2\,, \quad & & q_2 = \frac{c_1 c_2}{k}, \\ \text{resp. case (c)} \quad & p_1 = \frac{c}{k_1}\,, & q_1 = \frac{k_1 + k_2}{k_1 k_2}\,, \quad & & q_2 = \frac{c}{k_1 k_2}. \end{aligned}$$

The constants c_i, k_i or p_i cannot directly be derived from material constants. They must be fitted to reference data, e. g., from experiments or ERF flow simulations. Both the 3-parametric fluid and the 3-parametric solid models are popular substitutive models for viscoelastic materials such as polymers.

These models may represent the behavior of the ERF at small shear strain rates, i. e., for shear stresses less than the yield point. When combined with suitable models representing the phase of large shear stresses, e. g., the Bingham model, we expect a substitutive model of the damping behavior of an ERF shock absorber over the whole range of operation. Stanway et. al. [35] (Fig. 10(a)) use a simple spring according to elastic properties of the fluid and the accumulator. The damping characteristics are calculated by the simplified flow model mentioned earlier in this section. However, this approach obviously neglects the so-called viscous damping at the viscoelastic phase.

As depicted in Fig. 10(b) this problem is tackled straightforward with the model of Ehrgott and Masri [13,24]. Both the Bingham model and the 3-parametric fluid model have been arranged serially with satisfying results

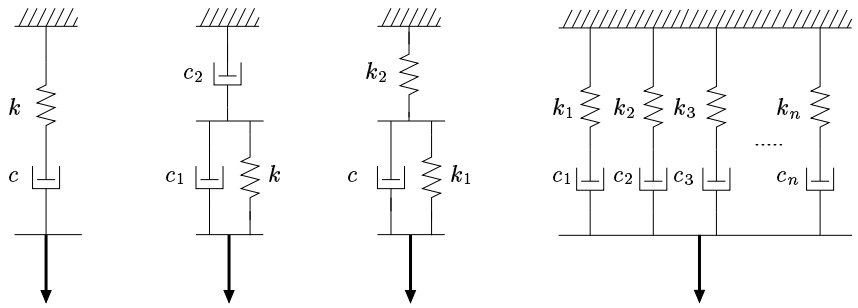

Fig. 9. Substitutive models for viscoelastic behavior: (a) conventional Maxwell model, (b) 3-parametric fluid model, (c) 3-parametric solid model, (d) general Maxwell model.

comparing simulation and measurement data. Another phenomenological model has been described by Powell [31] with a model containing a nonlinear spring and with parameters fitted to measurement data.

The approach of Spencer et.al. [33] is a completely phenomenological model. It takes into account the hysteresis within the force-velocity relation and is called the *augmented Bouc-Wen model* (Fig. 10(d)). It includes the largest number of parameters. The augmented Bouc-Wen model and the model of Ehrgott and Masri have been most well accepted. Transcribing the mechanical system into mathematical terms we obtain

$$\begin{aligned} (c_0 + c_1)\dot{s} &= c_1\dot{x} - \alpha z - k_0 s, \\ \dot{z} &= (A - \beta(1 + \operatorname{sgn}(\dot{s}z))z^2)\dot{s} \end{aligned} \tag{27}$$

which is a hysteresis operator with the inner variables s, z and constants c_0, c_1, k_0, α, β, and A. The acting force is

$$F = c_1(\dot{x} - \dot{s}) + k_1(x - x_0) \tag{28}$$

with further constants k_1 and x_0.

The augmented Bouc-Wen Model has been tested in the context of field dependence [34]. The characteristic parameters c_0, c_1 and α are modelled as linearly depending on the field strength including a time delay, i.e.,

$$\begin{aligned} p &= p_a + v\, p_b \\ \dot{v} &= \eta(u - v) \end{aligned} \tag{29}$$

where p is either one of c_0, c_1 or α. Furthermore, u denotes the actual field strength, while v stands for a virtual time delayed field strength depending on a constant η according to the known time delay of acting ERF devices.

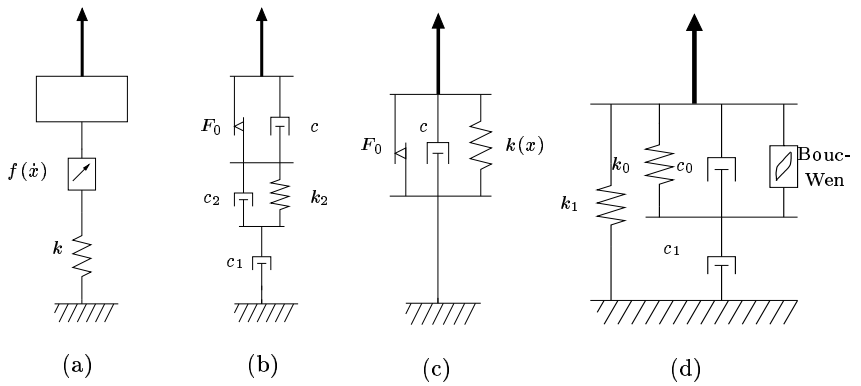

Fig. 10. Substitutive models of viscoelastic-plastic system behavior: (a) Peel, Stanway, Bullough; (b) Powell; (c) Ehrgott, Masri resp. Kamath, Wereley; (d) Spencer et. al.

In summary, all the described models include a priori unknown parameters which account for the uncertainty of unknown behavior of ERFs. Consequently some authors applied general functional approximation techniques, e. g., Chebyshev polynomials [16,27] or neural nets [29], to fit measurement data. However, it seems to be advantageous to use a priori knowledge about the system behavior for deriving model equations whose solutions behave similar to the fluid properties, i. e., taking the main properties of the physical system into account within the describing equations. One property is the stiff behavior of the dynamic equations [36] caused by the phase changes between viscoelastic and plastic mode. These phase changes occur very often at typical frequencies of operating automotive shock absorbers (about 50 Hz [25]).

However, to some extent ERF devices exhibit even more properties which are not included in the models described so far as a temperature dependence of the fluid's yield point and a dropping of the yield point with an increase in the frequency acting on the ERF device. Furthermore, some authors [29] believe that elastic properties of the ER fluids do not significantly affect the system behavior of an ERF shock absorber contrary to the results of other authors for magnetorheological fluids [33].

3.3 Control of ERF Dampers for Active Vehicle Suspension

The regulator problem for an ERF damper as part of an active vehicle suspension is to control the electric field in such a way that comfort and safety are *maximized* during the vehicle ride. For this purpose, *optimal* control methods must be investigated that take into account the nonlinear dynamical behavior of the ERF damper as well as of the vehicle itself.

Conventional regulator techniques for active suspension of vehicles are based on controlling the pressure of gas inside a cylinder or the flow of a vis-

cous fluid by a regulator valve. Commonly used control algorithms are only semi-active: The driver or a control unit selects the actual damper characteristic from several force-velocity relations of fixed damper settings corresponding to various ride levels of comfort or safety.

The technology of ER (or MR) fluids offers new control strategies. As already mentioned the electric field regulates the viscosity of the fluid within milliseconds. Hence, the flow through a gap acts as the flow through a continuously adjustable valve which can be opened or closed very fast and with almost no wear. It is possible in principle to adapt the damping rate within one cycle of a damper movement thus enabling fully active vehicle suspensions. In the sequel, an *optimal* damping force is investigated for active suspension of a quarter vehicle. The resulting ideal damping rate serves as a setpoint trajectory for the ERF damper.

The essential gains in shock absorber regulation are comfort and safety of the vehicle ride which are antagonistic gains. If, as usual, the objective is modeled as a weighted sum of both objectives then the proper selection of the weights is an ambiguous problem that must be addressed.

Technically speaking the regulation is concerned with eliminating or decreasing the effect of street disturbances. Especially the excitations close to eigenfrequencies of the vehicle body have to be avoided as well as frequencies which lead to unhealthy vibrations of the vehicle passengers. These effects are observed by the history of the sprung mass acceleration $\ddot{x}_a$ if a quarter car model is considered for the vehicle dynamics (Fig. 11). Furthermore the priority and, thus, the weights of comfort and safety depend on the current driving situation. E. g., driving safety has absolute priority in dangerous situations. This comes along with ensuring large values of the vertical wheel load forces which is necessary for a good maneuverability of a vehicle [1].

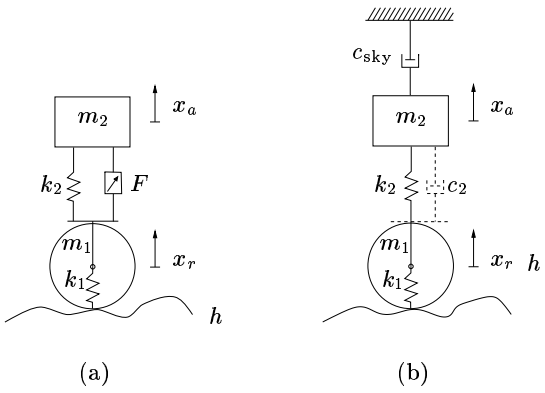

Fig. 11. Quarter car model with (a) a controllable damping force F and (b) the sky-hook assumption.

Fig. 11(b) depicts a possibility to avoid sprung mass oscillations with eigenfrequencies of a quarter car model (cf. [30]). The damping rate c_2 is adjusted as if a virtual damper c_{sky} would act with a constant proper damping rate. The resulting damping law is technically not realizable, but approximately included in common damping strategies. The outcome of this approach are different compression and decompression damping rates.

Since the *sky-hook* regulator is based on a heuristic approach, a better performance can be expected if *optimal* control techniques are applied based on a general problem formulation: A linear system behavior of the differential equations for the state variables $\mathbf{x}$ of the vehicle is considered

$$\dot{\mathbf{x}} = \mathbf{A}\mathbf{x} + \mathbf{B}\mathbf{u}, \quad \mathbf{x}(t_0) = \mathbf{x}_0 \tag{30}$$

with $\mathbf{x} \in \mathbb{R}^{n_x}$, $\mathbf{u} \in \mathbb{R}^{n_u}$, $\mathbf{A} \in \mathbb{R}^{n_x \times n_x}$, $\mathbf{B} \in \mathbb{R}^{n_x \times n_u}$. For the linear quadratic Bolza type objective

$$J[\mathbf{u}] = {\mathbf{x}_f}^{\mathrm{T}}\mathbf{Q}_f\mathbf{x}_f + \int_{t_0}^{t_f} \mathbf{x}^{\mathrm{T}}\mathbf{Q}\mathbf{x} + 2\mathbf{u}^{\mathrm{T}}\mathbf{S}\mathbf{x} + \mathbf{u}^{\mathrm{T}}\mathbf{R}\mathbf{u}\,\mathrm{d}t \tag{31}$$

with $\mathbf{x}_f = \mathbf{x}(t_f)$, a solution of the problem can be calculated straightforward solving the corresponding Riccati differential equation for $\mathbf{P} \in \mathbb{R}^{n_x \times n_x}$

$$\begin{aligned} &\dot{\mathbf{P}} + \mathbf{A}^{\mathrm{T}}\mathbf{P} + \mathbf{P}\mathbf{A} + \mathbf{Q} - (\mathbf{P}\mathbf{B} + \mathbf{S})\mathbf{R}^{-1}(\mathbf{B}^{\mathrm{T}}\mathbf{P} + \mathbf{S}^{\mathrm{T}}) = \mathbf{0} \\ &\mathbf{P}(t_f) = \mathbf{Q}_f. \end{aligned} \tag{32}$$

if no inequality constrains are active. A steady state problem, i.e., $\dot{\mathbf{P}} = \mathbf{0}$, $\mathbf{Q}_f = \mathbf{0}$ and $t_f \to \infty$ in (32), leads to an algebraic Riccati equation. Thus, the *optimal* feedback control $\mathbf{u}^*(\mathbf{x})$ is determined by

$$\mathbf{u}^* = -\mathbf{R}^{-1}(\mathbf{B}^{\mathrm{T}}\mathbf{P} + \mathbf{S}^{\mathrm{T}})\mathbf{x}^* \tag{33}$$

where $\mathbf{x}^*$ denotes the solution of

$$\begin{aligned} &\frac{\mathrm{d}}{\mathrm{d}t}\mathbf{x}^* = (\mathbf{A} - \mathbf{B}\mathbf{R}^{-1}(\mathbf{B}^{\mathrm{T}}\mathbf{P} + \mathbf{S}^{\mathrm{T}}))\mathbf{x}^* \\ &\mathbf{x}^*(t_0) = \mathbf{x}_0. \end{aligned} \tag{34}$$

However, it must be assumed that the system is stabilizable, $\mathbf{R}$ is positive definite, $\mathbf{Q} - \mathbf{S}\mathbf{R}^{-1}\mathbf{S}^{\mathrm{T}}$ is positive semidefinite and there are no limitations on the observability of $\mathbf{x}$. This method is well known as the *linear quadratic regulator* (LQR) and is popular in many fields of applications (cf. [26,28]).

A drawback of the previous approach is that the solution is only optimal with regard to a step disturbance at initial time. Although the LQR can be extended to a linear, time varying road disturbance $\mathbf{w}$ acting in the following way with $\mathbf{D} \in \mathbb{R}^{n_x \times n_w}$

$$\dot{\mathbf{x}} = \mathbf{A}\mathbf{x} + \mathbf{B}\mathbf{u} + \mathbf{D}\mathbf{w} \tag{35}$$

a desireable property of the regulator is to compensate *all* possible disturbances $\mathbf{w}$, particularly those which lead to unstable total systems.

With the state, control and disturbance variables $\mathbf{x}, \mathbf{u}$ and $\mathbf{w}$ as elements of suitable Hilbert spaces H_x, H_u, resp. H_w we now consider a given feedback control $\mathbf{u} = \mu(\mathbf{x}, t)$. The control law μ determines an operator

$$T_\mu : H_w \to H_x \tag{36}$$

which maps disturbances $\mathbf{w}$ onto solutions $\mathbf{x}$ of the state equations. With appropriate norms of the according Hilbert spaces a maximum norm of the operator T_μ is defined [4]

$$\|T_\mu\|_\infty = \sup_{w \in H_w} \frac{\|T_\mu\|_x}{\|w\|_w} \tag{37}$$

which is related to the values of disturbances ($\|.\|_x$ and $\|.\|_w$ are defined according to (40) and (41)). Decreasing the maximum value means to attenuate disturbance influence on the total system, so we have to find the control law μ^*, which yields an infimum for the worst case disturbance

$$\inf_\mu \|T_\mu\|_\infty = \phi^* \,, \tag{38}$$

i. e., the worst case is bounded simultaneously. Here the feasible controls μ are restricted implicitly, as a stable system is required. If there exists a solution μ^* of (38) we obtain the inequality

$$\|T_{\mu^*}(\mathbf{w})\|_x{}^2 \leq \phi^{*2} \|\mathbf{w}\|_w{}^2 \quad \text{for all} \quad \mathbf{w} \in H_w \tag{39}$$

as well as the uniqueness of μ^* (cf. [4]). Using the definition of the objective

$$J_\phi[\mu, \mathbf{w}] = \|T_\mu(\mathbf{w})\|_x{}^2 - \phi^2 \|\mathbf{w}\|_w{}^2 = J[\mu, \mathbf{w}] - \phi^2 \|\mathbf{w}\|_w{}^2 \tag{40}$$

and replacing $J[\mu, \mathbf{w}]$ by the objective from (31) leads to a zero-sum differential game with the expanded linear quadratic objective

$$J_\phi[\mathbf{u}, \mathbf{w}] = \mathbf{x}_f{}^{\mathrm{T}} \mathbf{Q}_f \mathbf{x}_f + \int_0^{t_f} \mathbf{x}^{\mathrm{T}} \mathbf{Q} \mathbf{x} + 2\mathbf{u}^{\mathrm{T}} \mathbf{S} \mathbf{x} + \mathbf{u}^{\mathrm{T}} \mathbf{R} \mathbf{u} - \phi^2 \mathbf{w}^{\mathrm{T}} \mathbf{w} \, \mathrm{d}t \,. \tag{41}$$

The first player chooses the control $\mathbf{u}$ to minimize the objective while the second player chooses the road disturbances $\mathbf{w}$ to maximize it. The solution defines the *best worst case*, i. e., what can be obtained at least with optimal control under the worst possible circumstances.

The solution of the H^∞ problem again reduces to the solution of the corresponding Riccati equation for $\mathbf{P}_\phi \in \mathbb{R}^{n_x \times n_x}$

$$\begin{aligned} &\dot{\mathbf{P}}_\phi + \mathbf{A}^{\mathrm{T}} \mathbf{P}_\phi + \mathbf{P}_\phi \mathbf{A} + \mathbf{Q} - \\ &\quad - \left[\mathbf{P}_\phi \left[\mathbf{B}\ \mathbf{D}\right] + \left[\mathbf{S}\ \mathbf{0}\right]\right] \begin{bmatrix} \mathbf{R}^{-1} & \mathbf{0} \\ \mathbf{0} & -\frac{1}{\phi^2} \end{bmatrix} \left[\begin{bmatrix} \mathbf{B}^{\mathrm{T}} \\ \mathbf{D}^{\mathrm{T}} \end{bmatrix} \mathbf{P}_\phi + \begin{bmatrix} \mathbf{S}^{\mathrm{T}} \\ \mathbf{0}^{\mathrm{T}} \end{bmatrix} \right] = \mathbf{0} \\ &\mathbf{P}_\phi(t_f) = \mathbf{Q}_f \end{aligned} \tag{42}$$

with a chosen $\phi > \phi^*$, and a zero matrix $\mathbf{0}$ of proper dimensions. The resulting control laws are

$$\mathbf{u}^* = \mu^*(t, \mathbf{x}_0) = -\mathbf{R}^{-1}(\mathbf{B}^{\mathrm{T}}\mathbf{P}_\phi + \mathbf{S}^{\mathrm{T}})\mathbf{x}^* \tag{43}$$

$$\mathbf{w}^* = \nu^*(t, \mathbf{x}_0) = \frac{1}{\phi^2}\mathbf{D}^{\mathrm{T}}\mathbf{P}_\phi\mathbf{x}^* \tag{44}$$

with the corresponding optimal state trajectory

$$\begin{aligned} \dot{\mathbf{x}}^* &= (\mathbf{A} - \mathbf{B}\mathbf{R}^{-1}(\mathbf{B}^{\mathrm{T}}\mathbf{P}_\phi + \mathbf{S}^{\mathrm{T}}) + \frac{1}{\phi^2}\mathbf{D}\mathbf{D}^{\mathrm{T}}\mathbf{P}_\phi)\mathbf{x}^* \\ \mathbf{x}^*(t_0) &= \mathbf{x}_0 \,. \end{aligned} \tag{45}$$

However, the existence of a solution to the Riccati equation is not guaranteed for the infimum ϕ^* if $\dot{\mathbf{P}} = \mathbf{0}$ [4]. Then only a suboptimal solution can be obtained for a $\phi > \phi^*$. Suboptimal solutions exist for sufficiently large ϕ because the solution of the LQR problem is obtained as $\phi \longrightarrow \infty$.

The numerical solution is obtained iteratively by solving a sequence of problems with decreased values of ϕ while all iterates must satisfy that the algebraic Riccati equation (42) is solvable and the controlled and disturbed systems are stable.

The H^∞ approach ensures *robust optimality* and is suitable for linear dynamical vehicle models such as quarter car models. However, several limitations exist: The calculation of the optimal damping force is unconstrained, although it is limited by the shock absorber properties in practice. For problems with a *nonlinear* objective or *nonlinear* dynamics or active state and control *constraints*, the numerical computation of the optimal feedback controller $\mathbf{u}^*(\mathbf{x})$ is only possible in very special cases. However, a nonlinear optimization technique may be applied to compute an approximation of the optimal open loop control $\mathbf{u}^*(t)$ of a nonlinear dynamical system subject to constraints in case of a given road disturbance [26].

3.4 Numerical Results

Optimal active suspension of the quarter car model depicted in Fig. 11(a) with $\mathbf{x} = (x_r, x_a, \dot{x}_r, \dot{x}_a)^{\mathrm{T}}$, $n_x = 4$, and $\mathbf{u} = F$, $n_u = 1$, is investigated using a controllable rheological fluid damper and comparing LQR- and H^∞-regulators.

The vehicle data consists of the spring constants $k_1 = 190\,\mathrm{kN/m}$, $k_2 = 16.812\,\mathrm{kN/m}$, the masses $m_1 = 59\,\mathrm{kg}$, $m_2 = 290\,\mathrm{kg}$. An uncontrolled conventional damper with the constant damping rate $c_2 = 3.0\,\mathrm{kNs/m}$ is used for comparison (cf. [1]). The controllable rheological fluid damper is described by the Bouc-Wen model of Fig. 10(d) and (27,29) with constants $c_{1a} = 1.0\,\mathrm{kNs/m}$, $c_{1b} = 20.0\,\mathrm{kNs/m}$, $c_{2a} = 1.2\,\mathrm{kNs/m}$, $c_{2b} = 21.5\,\mathrm{kNs/m}$, $\alpha_a = 1.0\,\mathrm{kN/m}$, $\alpha_b = 200\,\mathrm{kN/m}$, $k_0 = 50\,\mathrm{kN/m}$, $k_1 = 100\,\mathrm{kN/m}$, $A = 47.2$,

$\beta = 3.93 \cdot 10^6\,\mathrm{cm}^{-2}$ and $\eta = 100\,\mathrm{s}^{-1}$. The constants have been chosen according to the results of Spencer et. al. [34] and adapted to damping rates of common automotive shock absorbers.

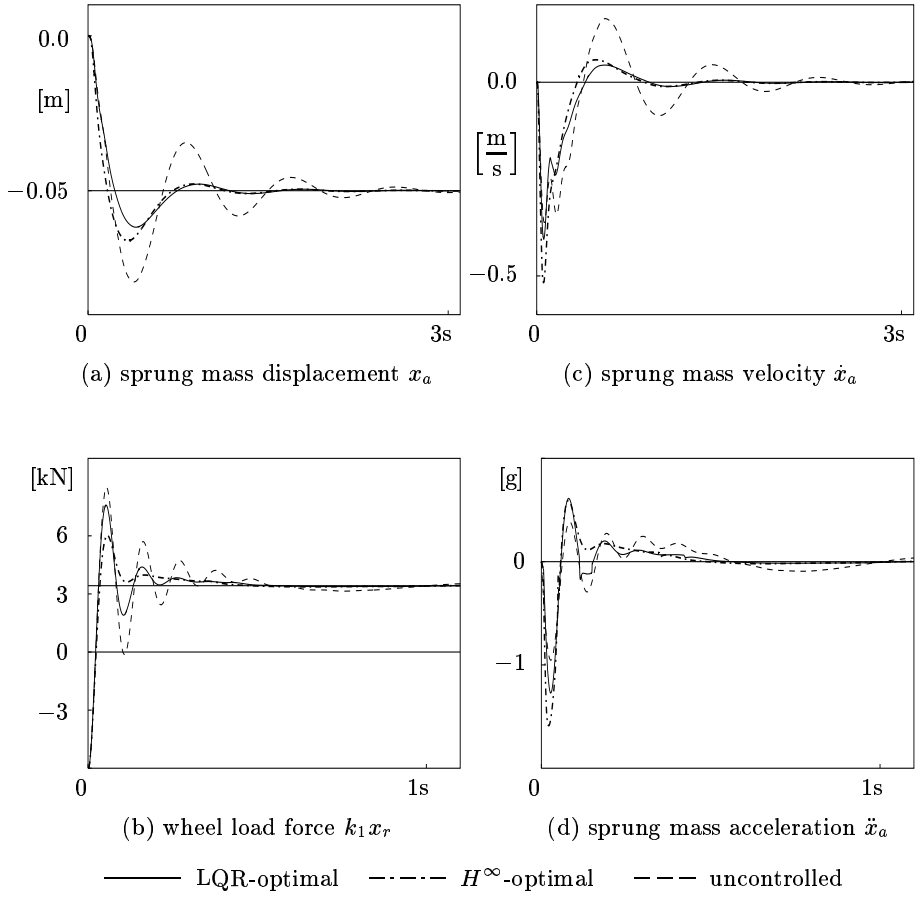

Fig. 12. State histories for the actively, LQR- and H^∞-controlled systems and for the passive suspension during the simulated ride with an initial fall off a step of 5 cm.

The objective to be minimized by the optimal damping force $F^* = \mathbf{u}^*$ is a weighted quadratic sum of the scaled sprung mass acceleration $\ddot{x}_a/g$ (cf. Fig. 11(a)), the scaled wheel load force $k_1 x_r/g(m_1+m_2)$, the force F/gm_2 and the state variables $x_i/x_{i,\max}$, $\dot{x}_i/\dot{x}_{i,\max}$, $i = a, r$ (cf. [26]). Uniform weights ($\mu = \mu_a = 1$) are chosen except for the states of the wheel, which are weighted

by $\mu_r = 1/10$ of the sprung mass states resulting in

$$J[F] = \int_0^\infty \mu \left(\frac{\ddot{x}_a}{g}\right)^2 + \mu \left(\frac{k_1 x_r}{g(m_1+m_2)}\right)^2 + \mu \left(\frac{F}{m_2 g}\right)^2 + \\ + \sum_{i=a,r} \mu_i \left(\frac{x_i}{x_{i,\max}}\right)^2 + \mu_i \left(\frac{\dot{x}_i}{\dot{x}_{i,\max}}\right)^2 \mathrm{d}t \,. \tag{46}$$

The histories of sprung mass displacement x_a and velocity $\dot{x}_a$ (Fig. 11(a)) for the uncontrolled system with a conventional passive damper and the actively, LQR- and H^∞-controlled systems for an initial step disturbance of 5 cm are depicted in Fig. 12. The numerical solutions have been obtained using MATLAB. A comparison of the wheel load forces is also given which are indicators for driving safety. If the wheel load becomes less or equal to zero then the vehicle is not maneuverable. On the other hand, the sprung mass acceleration $\ddot{x}_a$ is a measure of driving comfort. Obviously, an increase in safety, i. e., of the wheel load forces, comes for the price of an increased sprung mass acceleration, i. e., a decrease in comfort.

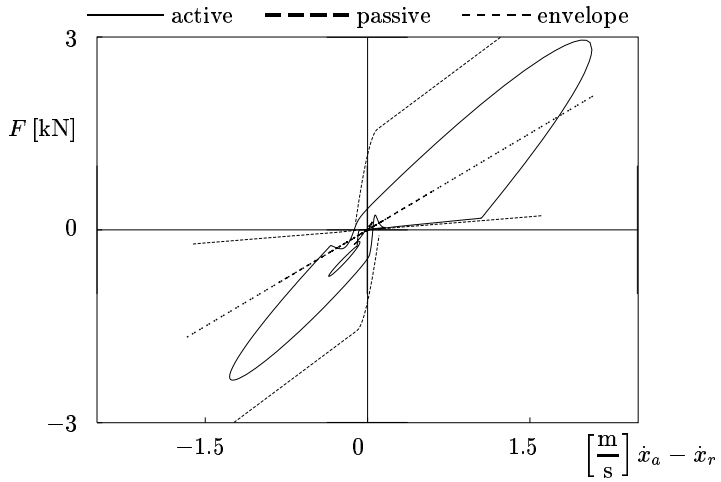

Fig. 13. Force-velocity graph of the actively LQR-controlled rheological fluid damper and the conventional passive damper during the simulated ride.

Actually, we are interested in the strength of the electric field u of (29)[1], which affects the viscosity of the damper. For this purpose, an extension of the approach of [33] to adjust the current damping force F to the computed

[1] Please note the difference between u and $\mathbf{u}$.

optimal damping force F^* is applied

$$u = \begin{cases} \min\left(u_{\max}, \left|\frac{F^*-F}{F_{\text{scal}}}\right| \left|\frac{F}{F_{\text{scal}}}\right|\right), & \text{if} \quad |F| < |F^*|, FF^* > 0, \\ u_{\min}, & \text{otherwise.} \end{cases} \tag{47}$$

with a proper scaling force (here $F_{\text{scal}} = 10^2\text{N}$) and the scaled values $u_{\max} = 1$ and $u_{\min} = 0$.

The force-velocity relation of the LQR-controlled rheological fluid damper model during the simulated ride is depicted in Fig. 13 in comparison with the passive damper demonstrating the innovative potential of optimally controlled electrorheological fluid dampers for active suspension of vehicles.

References

1. Alleyne, A., Hedrick, J. K.: Nonlinear adaptive control of active suspensions. IEEE Transactions on Control Systems Technology **3**, 1 (1995) 94–101
2. Atkin, R. J., Shi, X., Bullough, W. A.: Solutions of the constitutive equations for the flow of an electrorheological fluid in radial configuations. J. Rheology **35** (1991) 1441–1461
3. Backé, W., Fees, G., Murrenhoff, H.: Innovative Fluidtechnik - Hochdynamischer Servoantrieb mit elektrorheologischen Flüssigkeiten. o+p Ölhydraulik und Pneumatik **41** (1997) 11–12
4. Başar, T., Bernhard, P.: H^∞-Optimal Control and Related Minimax Design Problems: A Dynamic Game Approach. Birkhäuser, Boston (1991)
5. Bayer AG: Provisional Product Information. Rheobay TP AI 3565 and Rheobay TP AI 3566. Bayer AG, Silicones Business Unit, No. AI 12601e, Leverkusen (1997)
6. Bayer AG: Technology based on ERF. Rheobay for applications in fluid mechatronics (in cooperation with IFAS, RWTH Aachen, and Carl Schenck AG, Darmstadt). Bayer AG, Silicones Business Unit, No. AI 12666d+e, Leverkusen (1997)
7. Bayer AG and Carl Schenck AG: Active ERF-Vibrationdamper (a joint development by Carl Schenck AG and Bayer AG). Bayer AG, Silicones Business Unit, No. AI 12668d+e, Leverkusen/Darmstadt (1998)
8. Bird, B., Armstrong, R., Hassager, O.: Dynamics of Polymeric Liquids. J. Wiley and Sons, New York (1987)
9. Bonnecaze, R., Brady, J.: Dynamic simulation of an electrorheological fluid. J. Chem. Phys. **96** (1992) 2183–2202
10. Bonnecaze, R., Brady, J.: Yield stresses in electrorheological fluids. J. Rheol. **38** (1992) 73–115
11. Butz, T., von Stryk, O.: Modelling and simulation of rheological fluid devices. Preprint SFB-438-9911, Sonderforschungsbereich 438, Technische Universität München – Universität Augsburg (1999) 37 p.
12. Duvaut, G., Lions, J.: Inequalities in Mechanics and Physics. Springer, Berlin-Heidelberg-New York (1976)
13. Ehrgott, R. C., Masri, S. F.: Modelling the oscillatory dynamic behavior of electrorheological materials in shear. Smart Mat. Struct. **1** (1992) 275–285

14. Engelmann, B., Hiptmair, R., Hoppe, R.H.W., Mazurkevitch, G.: Numerical simulation of electrorheological fluids based on an extended Bingham model. Computing and Visualization in Science (submitted 1999)
15. Filisko, F.: Overview of ER technology. In: Progress in ER Technology, (Havelka, K.; ed.), Plenum Press, New York (1995)
16. Gavin, H. P., Hanson, R. D., Filisko, F. E.: Electrorheological dampers, Part I: Analysis and design. J. Appl. Mech. **63** (1996) 669–675
17. Gavin, H. P., Hanson, R. D., Filisko, F. E.: Electrorheological dampers, Part II: Testing and modeling. J. Appl. Mech. **63** (1996) 676–682
18. Glowinski, R., Le Tallec, P.: Augmented Lagrangian and Operator-Splitting Methods in Nonlinear Mechanics. SIAM Studies in Applied Mathematics **9** (1989)
19. Glowinski, R., Lions, J.L., Trémolières, R.: Numerical Analysis of Variational Inequalities. North-Holland, Amsterdam (1981)
20. Hartsock, D., Nowak, R., Chaundy, G.: ER fluid requirements for automotive devices. J. Rheol. **35** (1991) 1305–1326
21. Janocha, H., Rech, B., Bölter, R.: Practice-relevant aspects of constructing ER fluid actuators. Int. J. Modern Physics B **10** (1996) 3243–3255
22. Kamath, G. M., Hurt, M. K., Wereley, N. M.: Analysis and testing of Bingham plastic behavior in semi-active electrorheological fluid dampers. J. Appl. Mech. **63**c (1996) 676–682
23. Kamath, G. M., Wereley, N. M.: System identification of ER fluid dampers using a nonlinear mechanisms-based model. Paper No. SPIE-2717-46, 1996 SPIE Conference on Smart Materials and Structures, 25-29 February, San Diego, CA (1996)
24. Kamath, G. M., Wereley, N. M.: A nonlinear viscoelastic-plastic model for electrorheological fluids. Smart Mat. Struct. **6** (1997) 351–359
25. Kortüm, W., Lugner, P.: Systemdynamik und Regelung von Fahrzeugen. Springer-Verlag, Berlin (1994)
26. Koslik, B., Rill, G., von Stryk, O., Zampieri, D.: Active suspension design for a tractor by optimal control methods. Preprint SFB-438-9801, Sonderforschungsbereich 438, Technische Universität München – Universität Augsburg (1998) 23 p.
27. McGlamroch, N. H., Gavin, P. G.: Closed loop structural control using electrorheological dampers. Proc. American Control Conference (1995) 4173–4177
28. Levine, W. S. (ed.): The Control Handbook. CRC Press, Boca Raton (1996)
29. Makris, N., Burton, S. A., Taylor, D. P.: Modelling the response of ER damper: Phenomenology and emulation. J. Eng. Mech. (1996) 897–906
30. Mitschke, M.: Dynamik der Kraftfahrzeuge, Band B: Schwingungen. 3rd ed., Springer-Verlag (1993)
31. Powell, J. A.: Modelling the oscillatory response of an electrorheological fluid. Smart Mat. Struct. **3** (1994) 416–438
32. Rajagopal, K., Wineman, A.: Flow of electrorheological materials. Acta Mechanica **91** (1992) 57–75
33. Spencer Jr., B. F., Dyke, S. J., Sain, M. K., Carlson, J. D.: Modeling and control of magnetorheological dampers for seismic response reduction. Smart Mat. Struct. **5** (1996) 565–575
34. Spencer Jr., B. F., Dyke, S. J., Sain, M. K., Carlson, J. D.: Phenomenological model of a magnetorheological damper. J. Engrg. Mech., ASCE. **123** (1997) 230–238

35. Stanway, R., Peel, D. J., Bullough, W. A.: Applications of electro-rheological fluids in vibration control: A survey. Smart Mat. Struct. **5** (1995) 464–482
36. Stoer, J., Bulirsch, R.: Introduction to Numerical Analysis. 2nd ed., Springer-Verlag, Berlin (1993)
37. Wendt, E., Büsing, K.W.: Properties of a new generation of non-abrasive and water-free electrorheological fluids. Preprint. Bayer AG, Silicones Business Unit, Leverkusen (1997)
38. Whittle, M.: Computer simulation of an electrorheological fluid. J. Non-Newton. Fluid Mech. **37** (1990) 233–263
39. Whittle, M., Atkin, R.J., Bullough, W.: Fluid dynamic limitations on the performance of an electrorheological clutch. J. Non-Newton. Fluid Mech. **57** (1995) 61–81